Available online at www.sciencedirect.com
SCIENCE DIRECT®
Journal of Nuclear Materials 349 (2006) 167–177
journal of nuclear materials
www.elsevier.com/locate/jnucmat

Thermal conductivity and acid dissolution behavior of $MgO–ZrO_2$ ceramics for use in LWR inert matrix fuel ☆

P.G. Medvedev *, M.J. Lambregts, M.K. Meyer

Idaho National Laboratory, Nuclear Fuels and Materials Department, Materials and Fuels Complex, P.O. Box 1625, MS 6000, Idaho Falls, ID 83403, USA

Received 25 April 2005; accepted 21 October 2005

Abstract

Dual-phase $MgO–ZrO_2$ ceramics are proposed for use in inert matrix fuel for disposition of plutonium and minor actinides in existing light water reactors. The concept for use of this composite material was developed with the intent to capitalize on the known advantages of the composite's constituents: high thermal conductivity of MgO, and stability of ZrO_2 in LWR coolant. The study presented in this paper addressed the thermal conductivity and nitric acid solubility of $MgO–ZrO_2$ ceramics. Thermal analysis, based on experimental and analytical techniques, established that the product of all investigated compositions has the thermal conductivity superior to that of UO_2. Nitric acid dissolution experiments showed that only the free MgO phase dissolves in the nitric acid, leaving behind a porous pellet consisting of a ZrO_2-based solid solution.
Published by Elsevier B.V.

PACS: 28.41.Bm; 81.05.Je; 81.05.Mh; 28.41.Kw

1. Introduction

Dual-phase $MgO–ZrO_2$ ceramics are proposed for use in inert matrix fuel (IMF) for disposition of plutonium and minor actinides in existing light water reactors (LWR). The concept for use of this composite material was developed with the intent to capitalize on the known advantages of the composite's constituents: the high thermal conductivity of MgO, and the stability of ZrO_2 in LWR coolant. Prior experiments [1,2] performed at Argonne National Laboratory West were dedicated to fabrication, characterization and hydration resistance assessment of $MgO–ZrO_2$ compositions containing 30–60 wt% of MgO and up to 7 wt% of Er_2O_3 (a potential neutron poison). The ceramics were found to consist of two phases: a cubic ZrO_2-based solid solution and a pure cubic MgO (free MgO phase). The amount of MgO dissolved in the ZrO_2-based cubic solution phase was 13–17 mol.%. The Er_2O_3 dopant preferentially dissolved in the ZrO_2 phase. Limited degradation of the ceramics in static deionized water at 300 °C and 8.59 MPa occurred due to the hydration of the free MgO phase. Normalized

☆ Work supported by the Advanced Fuel Cycle Initiative of the US Department of Energy under contract no. W-31-109-ENG-38.
* Corresponding author. Tel.: +1 208 533 7199; fax: +1 208 533 7863.
E-mail address: pavel.medvedev@inl.gov (P.G. Medvedev).

0022-3115/$ - see front matter Published by Elsevier B.V.
doi:10.1016/j.jnucmat.2005.10.009

mass loss rate (NMLR), used as a quantitative indicator of degradation, was found to decrease exponentially with ZrO_2 content in the ceramics. The normalized mass loss rates for the MgO–ZrO_2 ceramics containing 30, 40, 50, and 60 wt% of MgO were 0.000131, 0.000595, 0.00256, and 0.00688 g/cm^2/h, respectively.

This paper describes results of further testing of MgO–ZrO_2 ceramics. Recognizing that thermal conductivity is one of the most important properties of nuclear fuels, a study aimed at assessing the thermal conductivity of MgO–ZrO_2 ceramics was carried out. Thermal conductivity was derived from thermal diffusivity measured by a laser flash method in the 200–1200 °C temperature range, measured density, and heat capacity calculated using the rule of mixtures. Furthermore, acid dissolution behavior of MgO–ZrO_2 ceramics was investigated experimentally to assess the possibility of reprocessing the IMF based on an MgO–ZrO_2 matrices.

2. Thermal analysis

2.1. Thermal diffusivity measurement

2.1.1. Experimental procedure

An experimental procedure described elsewhere [3] was followed. The procedure is based on delivering a pulse of thermal energy to one face of the analyzed sample and monitoring the temperature rise of the opposite face. The thermal diffusivity, α (cm^2/s) is determined from sample thickness L (cm), and the time elapsed from the moment when the pulse of thermal energy is delivered to the moment when the temperature of the opposite face of the sample reaches half of its maximum $t_{1/2}$ (s):

$$\alpha = \frac{0.13879L^2}{t_{1/2}}. \quad (1)$$

A Flashline 5000 Thermal Properties Analyzer (Anter Corporation, Pittsburg, PA) was utilized in this work. The apparatus employs a neodymium/glass laser as a source of thermal energy. The temperature rise of the sample is monitored by a solid-state infrared detector. Measurement and data collection are fully automated, and up to six samples can be analyzed in a batch.

The composition of ceramics tested in this work is given in Table 1. A detailed description of the ceramic pellet fabrication and characterization was reported earlier [1]. In addition, Table 1 includes the volume percent of free MgO present in the sample. This number was determined by subtracting the amount of MgO dissolved in the ZrO_2 phase from the total amount of MgO present in the powder mixture used in ceramic fabrication. The amount of MgO dissolved in the ZrO_2 phase was determined by energy dispersive spectroscopy and reported earlier [1]. Side-by-side comparison of the microstructures of ceramics with different compositions is shown in Fig. 1. As evident from Fig. 1 and Table 1, the amount of free MgO phase increases with the increase of MgO content in the ceramic, leading to an expectation of higher thermal conductivity in the MgO-rich compositions.

The measurements were performed on two sets of disk-shaped test specimens. The specimens included in the first set were 2 mm thick, while the specimens included in the second set were 3 mm thick. The diameter of specimens in both sets was 6.25–6.28 mm. They were machined from as-sintered ceramic pellets by an external contractor (International Ceramics Engineering, Worcester, MA). Machined discs were coated on both faces with a very thin layer of palladium using a Hummer sputter coater (Anatech LTD, Denver, NC). A second coat of colloidal graphite was then sprayed-on to prevent possible reflection of the laser beam by the

Table 1
Composition and density of ceramic samples

Sample designation	Composition, wt%			Density, g/cm^3	Phases present in the product		
	MgO	ZrO_2	Er_2O_3		Porosity, vol.%	MgO, vol.%	ZrO_2-based solid solution, vol.%
40/60	40	60	0	4.61	0.43	46.80	52.77
50/50	50	50	0	4.39	0.45	57.94	41.61
60/40	60	40	0	4.19	0.23	67.94	31.83
40/60-Er	37.2	55.8	7	4.76	0.63	44.92	54.45
50/50-Er	46.5	46.5	7	4.54	0.87	55.81	43.32
60/40-Er	55.8	37.2	7	4.33	1.14	65.54	33.32

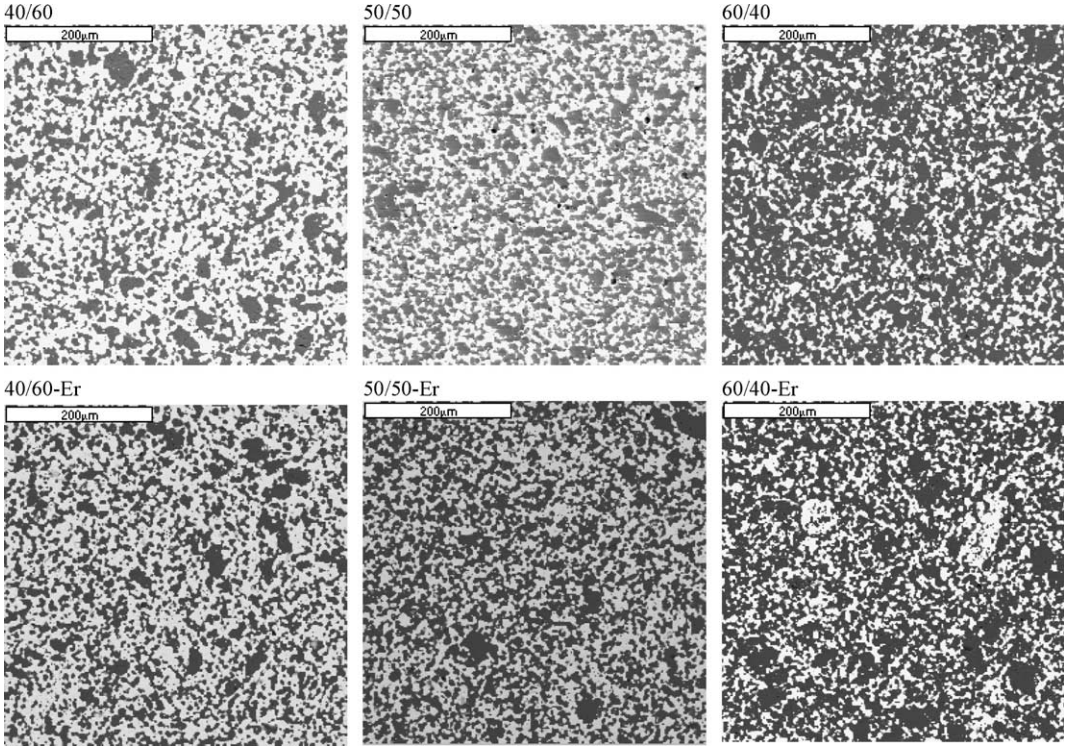

Fig. 1. Side-by-side comparison of the microstructures of ceramics with different compositions. Dark area: MgO; light area: ZrO_2-based solid solution.

palladium coating. The measurements were performed in a flowing argon atmosphere.

For each analyzed sample multiple attempts to measure the thermal diffusivity were performed at each given temperature. Spurious measurements caused by either excessive or insignificant laser power were identified by examining the raw data and the temperature rise curves. Results of such measurements were excluded from further consideration.

2.1.2. Results of thermal diffusivity measurements

To account for the conduction heat losses to the sample holders and for the radiation heat losses from the sample surfaces, the Cowan cooling curve correction [3] was used. The correction was performed utilizing the software provided by the manufacturer of the Flashline 5000 Thermal Properties Analyzer (Anter Corporation, Pittsburg, PA). Due to this correction, the reported values were 5–25% lower then the raw values determined from the temperature rise data using Eq. (1). The difference due to the correction increased with an increase of temperature, which indicated that more heat is lost by conduction and radiation at higher measurement temperatures. An illustration of how the Cowan correction has affected the data is shown in Fig. 2.

Third order polynomial fits of the corrected thermal diffusivity data are shown in Figs. 3 and 4. The polynomial fits were generated by conducting a least squares linear regression analysis. The resulting equation is as follows:

$$\alpha = aT^3 + bT^2 + cT + d, \tag{2}$$

where α is thermal diffusivity in s/cm^2; T is temperature in degrees °C; and a, b, c, and d are coefficients. The coefficients for specific compositions are listed in Table 2.

The thermal diffusivity of the binary and ternary systems investigated in this work appears to be driven by the temperature and composition. The decrease of thermal diffusivity with temperature is obvious. However, the degradation of thermal diffusivity with temperature is less pronounced at temperatures above 600 °C. To account for this behavior, the preference was given to the third degree polynomial fits of thermal diffusivity versus temperature, rather than the commonly used inverse temperature fits.

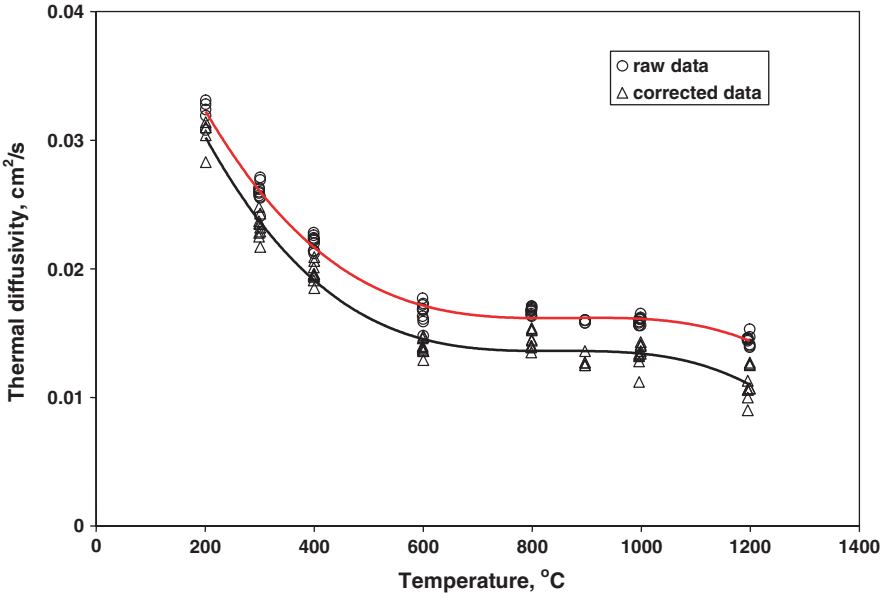

Fig. 2. Effect of Cowan cooling correction on the thermal diffusivity data. The data for the 50/50 composite is shown.

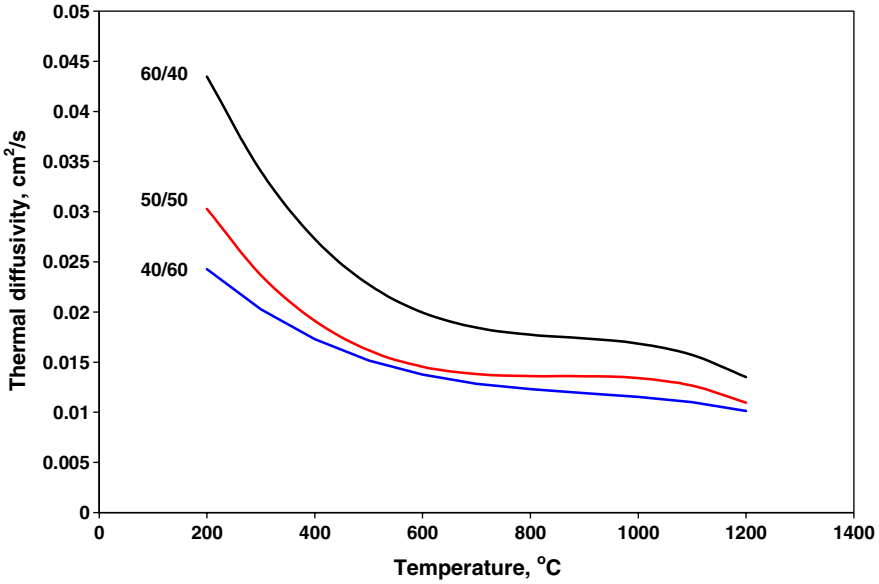

Fig. 3. Effect of MgO content on thermal diffusivity of the binary compositions.

Ronchi et al. [4] explained the increase of thermal conductivity in heterogeneous ZrO_2-actinide ceramics composites by the increase in the interface conductance between two phases at high temperature. According to Ronchi et al. [4], the latter is due to the difference in the thermal expansion between two phases. This explanation may be valid for the systems examined in this work, since MgO is known to have significantly higher thermal expansion than ZrO_2.

To further illustrate the discontinuity in thermal diffusivity behavior, the inverse thermal diffusivity versus temperature is plotted in Fig. 5. The dependence is clearly linear below 600 °C, but the linearity no longer exists above 600 °C.

With respect to the compositional dependence of thermal diffusivity, it was found that thermal diffusivity increases with the increase of MgO content in the ceramics. This trend was observed for both

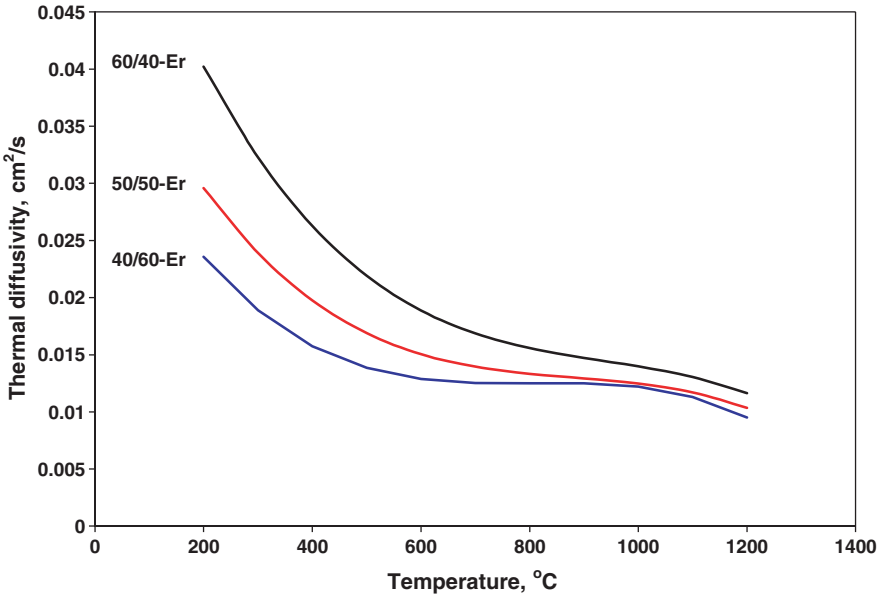

Fig. 4. Effect of MgO content on thermal diffusivity of the ternary compositions.

Table 2
Coefficients of the polynomial fits of the thermal diffusivity data

Composition	*a*	*b*	*c*	*d*
40/60	-2.862515×10^{-11}	7.754661×10^{-8}	-7.348286×10^{-5}	0.03610923
50/50	-6.128045×10^{-11}	1.559863×10^{-7}	-1.322989×10^{-4}	0.05099793
60/40	-7.883493×10^{-11}	2.057700×10^{-7}	-1.824712×10^{-4}	0.07238260
40/60-Er	-5.089583×10^{-11}	1.228926×10^{-7}	-9.856508×10^{-5}	0.03877326
50/50-Er	-4.426592×10^{-11}	1.170406×10^{-7}	-1.069412×10^{-4}	0.04664686
60/40-Er	-5.055004×10^{-11}	1.423967×10^{-7}	-1.409894×10^{-4}	0.06312453

binary and ternary compositions. The superposition of thermal diffusivity plots obtained for different concentrations of MgO illustrates this trend (Figs. 3 and 4). For clarity, only polynomial fits, and not the entire data sets are shown.

Er_2O_3 doping in the amount of 7 wt% had a minor effect on the thermal diffusivity of ceramic composites, which is illustrated in Fig. 6. According to Table 1, 7 wt% Er_2O_3 doping resulted in a less than 2% decrease of the volume percent of free MgO phase, thus having a minor impact on thermal diffusivity. It has been noted by Degueldre et al. [5] that doping of ZrO_2 with rare earth and actinide oxides including plutonia results in a large decrease of thermal conductivity of ZrO_2-based inert matrix fuel. Therefore, the minor effect of Er_2O_3 doping on the thermal diffusivity of MgO–ZrO_2 composites is a notable advantage over ZrO_2-based inert matrix fuels. This phenomenon is explained by a favorable phase distribution that takes place when MgO–ZrO_2 composite is doped with Er_2O_3. As it was established [1] by SEM and XRD, Er_2O_3 dissolves completely in the ZrO_2 phase, leaving the MgO phase uncontaminated. The latter implies that the thermal transport properties of MgO are unaffected by Er_2O_3 doping. It is understood that Er_2O_3 doping is likely to reduce the thermal diffusivity of the ZrO_2 phase; however, as evident from Fig. 6, the net effect of doping on the thermal diffusivity of the composite is not significant.

2.2. Heat capacity determination

Heat capacity was determined using the rule of mixtures (Neumann–Kopp law) from the published heat capacity data of MgO, ZrO_2, and Er_2O_3. Based on this rule, the heat capacity of a ceramic composite can be determined as a weighted sum of heat capacities of all components:

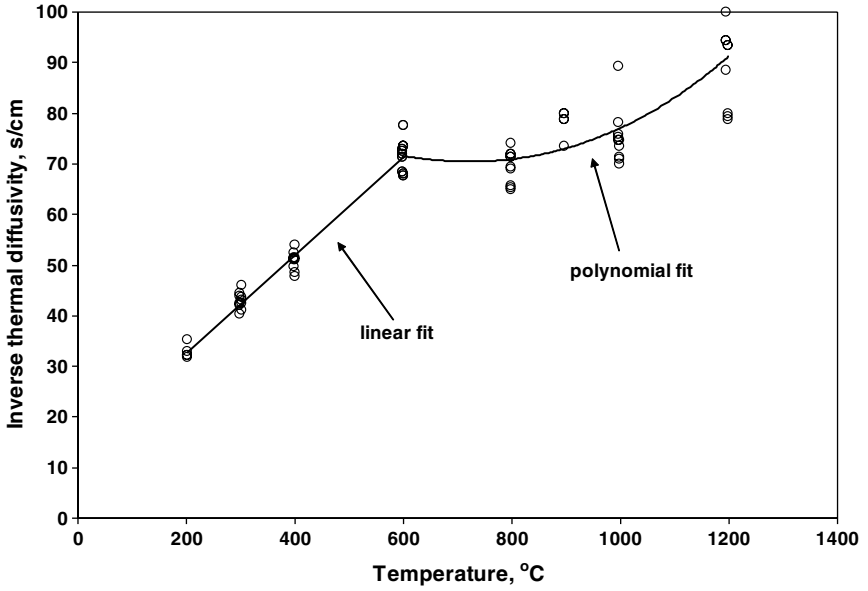

Fig. 5. Inverse thermal diffusivity versus temperature. The 50/50 composite data is shown.

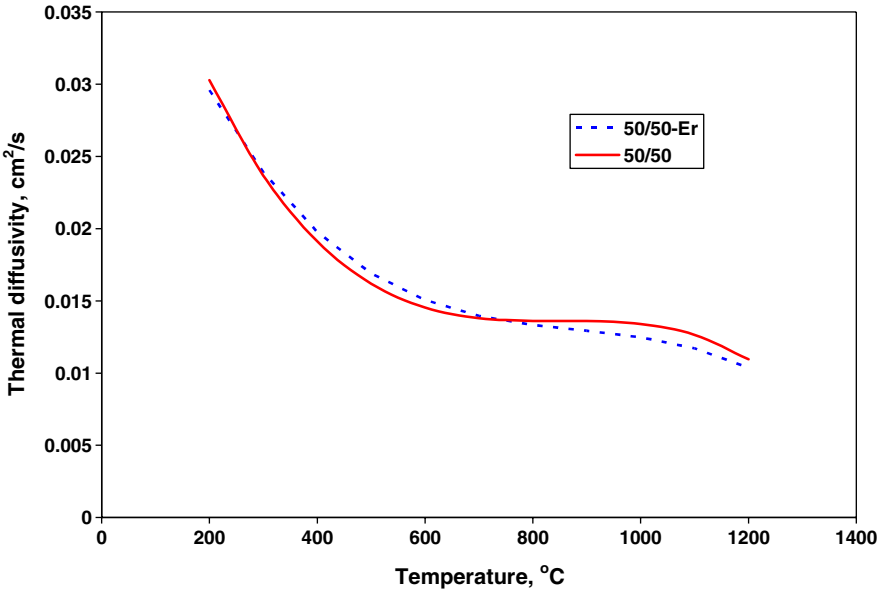

Fig. 6. Effect of Er_2O_3 doping on thermal diffusivity.

$$C_{\text{composite}} = aC_{\text{MgO}} + bC_{\text{ZrO}_2} + cC_{\text{Er}_2\text{O}_3}, \quad (3)$$

where a, b, and c are the weight fractions of the components in the ceramic, and C, J/(kg K) is the heat capacity of the individual components.

The following equations defining the temperature dependence of the heat capacity of individual components were used.

For MgO:

$$C_{\text{MgO}} = 47.25995 + 5.681621 \times 10^{-3}T - 8.72665 \times 10^{-7}T^2 + +1.043 \times 10^{-10}T^3 - 1.053955 \times 10^{6}T^{-2}, \quad (4)$$

where T is temperature in Kelvin, and C is heat capacity in J/K mole.

For ZrO_2:

$$C_{ZrO_2} = 69.20001 + 8.54829 \times 10^{-3}T - 8.62921 \times 10^{-7}T^2 + +2.46374 \times 10^{-10}T^3 - 1.382767 \times 10^{6}T^{-2}, \quad (5)$$

where T is temperature in Kelvin, and C is heat capacity in J/K mole.

For Er_2O_3:

$$C_{Er2O3} = 30.93 + 7.8 \times 10^{-4}T - 4.65 \times 10^{5}T^{-2}, \quad (6)$$

where T is temperature in Kelvin, and C is heat capacity in calorie/K-mole.

The equations for MgO and ZrO_2 were recommended by Ottaviani [6] based on the published data from NIST-JANAF Thermochemical Tables [7]. The equation for Er_2O_3 was developed by Tsagareishvili and Gvelesiani [8] based on the experimental measurements.

Based on these equations, the temperature dependence of the heat capacity for the ceramic compositions under investigation was calculated using the rule of mixtures. Necessary unit conversions were made to insure consistency of the units between Eq. (3) and Eqs. (4)–(6). The values of heat capacity were used later for thermal conductivity determination.

2.3. Thermal conductivity determination

Thermal conductivity was determined from thermal diffusivity, heat capacity, and density of the ceramics according to the following equation:

$$k = \alpha\rho C, \quad (7)$$

where α is thermal diffusivity in s/m^2, ρ is density in kg/m^3, and C is specific heat in J/kg K. The values of the thermal conductivity calculated from the measured thermal diffusivity, corrected for the heat losses using Cowan correction, measured density and estimated heat capacity are plotted in Figs. 7 and 8. The literature values [9] for fully dense UO_2 are included for comparison.

The plots in Figs. 7 and 8 represent the third order polynomial fits of the calculated data. The polynomial fits were generated by conducting a least squares linear regression analysis. The resulting equation is as follows:

$$k = aT^3 + bT^2 + cT + d, \quad (8)$$

where k is thermal conductivity in W/m K; T is temperature in °C; and a, b, c, and d are coefficients. The coefficients for specific compositions are listed in Table 3.

Thermal conductivity results shown in Figs. 7 and 8, particularly the comparison with UO_2, speak strongly in support of use of MgO–ZrO_2 ceramics as a matrix in IMF.

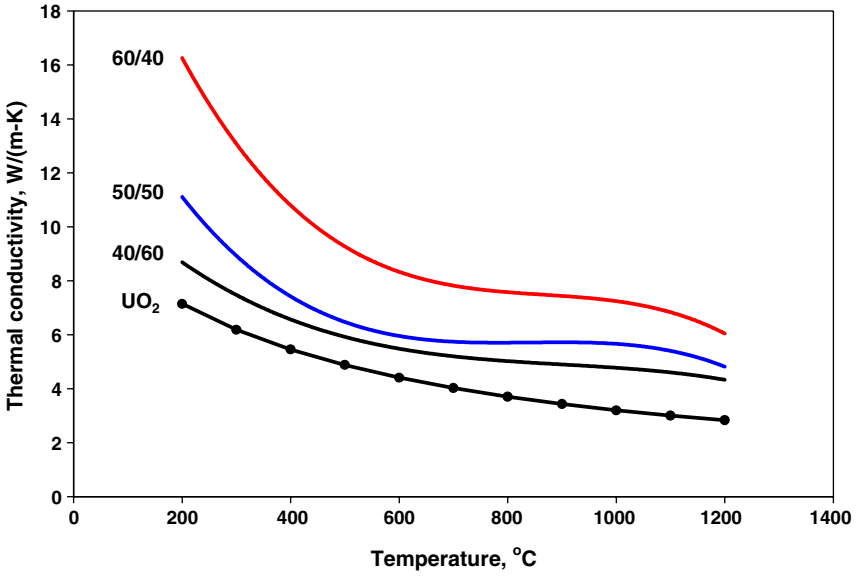

Fig. 7. Thermal conductivity of binary MgO–ZrO_2 ceramics with different compositions calculated using Eq. (7) shown in comparison with fully dense UO_2 [9].

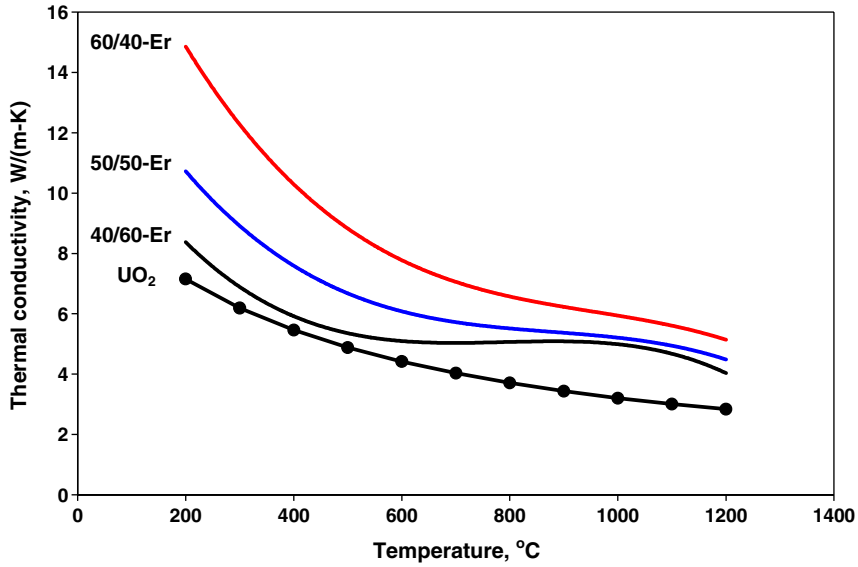

Fig. 8. Thermal conductivity of ternary MgO–ZrO_2–Er_2O_3 ceramics with different compositions calculated using Eq. (7) shown in comparison with fully dense UO_2 [9].

Table 3
Coefficients of the polynomial fits of the thermal conductivity versus temperature

Composition	a	b	c	d
40/60	-0.8575×10^{-8}	2.3248×10^{-5}	-2.2157×10^{-2}	12.26175
50/50	-2.1058×10^{-8}	5.3122×10^{-5}	-4.4452×10^{-2}	18.05258
60/40	-2.6855×10^{-8}	6.9733×10^{-5}	-6.1654×10^{-2}	26.02313
40/60-Er	-1.7461×10^{-8}	4.1348×10^{-5}	-3.2196×10^{-2}	13.29746
50/50-Er	-1.4169×10^{-8}	3.7292×10^{-5}	-3.4078×10^{-2}	16.16135
60/40-Er	-1.5390×10^{-8}	4.4094×10^{-5}	-4.4982×10^{-2}	22.21508

3. Experiments to assess the feasibility of reprocessing of MgO–ZrO_2-based IMF

Experiments to assess the feasibility of reprocessing of MgO–ZrO_2-based IMF were carried out. Dissolution of ceramic samples in nitric acid was attempted. Three ceramic samples (compositions 40/60, 50/50 and 60/40) in the form of discs 1–2 mm thick and 10–11 mm in diameter were exposed to the concentrated nitric acid. A hot plate equipped with a magnetic stirrer was utilized to keep the temperature of the acid at ~55 °C and provide continuous stirring. The dissolution was conducted in a glass flask fitted with a reflux condenser.

Periodically samples were removed from the acid rinsed with water, dried at 80 °C and weighed. The mass of the samples and the time elapsed since the start of the dissolution were logged. The resulting trend showing the evolution of sample weight loss with time is presented in Fig. 9.

No appearance changes were registered during a visual inspection of the samples exposed to the nitric acid. Despite significant mass loss the samples' geometrical dimensions remained unchanged as well. The sample weight loss at the end of the dissolution was equal 35.8%, 46.5%, 57.4% for 40/60, 50/50 and 60/40 compositions, respectively. Because the weight percent lost during dissolution was very close to the weight percent of crystalline MgO present in the samples (Table 1), and recognizing MgO's high solubility in the nitric acid, it was concluded that the attempt to dissolve the said ceramic compositions resulted in a selective leaching of the crystalline MgO phase. The second phase, MgO–ZrO_2 solid solution, failed to dissolve in any appreciable amount.

SEM examination of an acid-digested ceramic pellet (50/50 composition) yielded images shown in Fig. 10. Energy dispersive spectroscopy established that the light phase shown in Fig. 10 is MgO–ZrO_2 solid solution. The dark phase is porosity

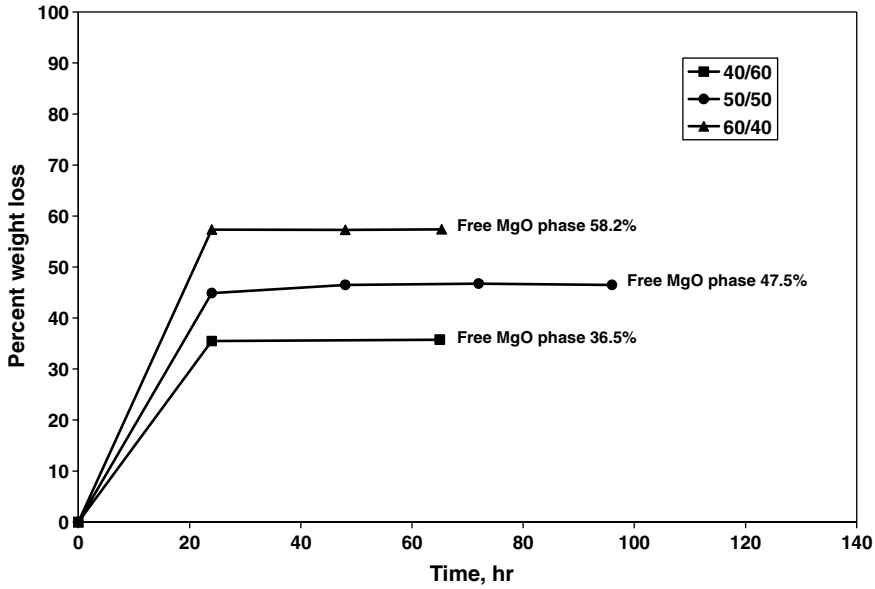

Fig. 9. Evolution of sample weight loss with time during sample dissolution in nitric acid. Free MgO content of the ceramic compositions is included to emphasize the agreement between the final weight loss and the free MgO content in the as-fabricated ceramics.

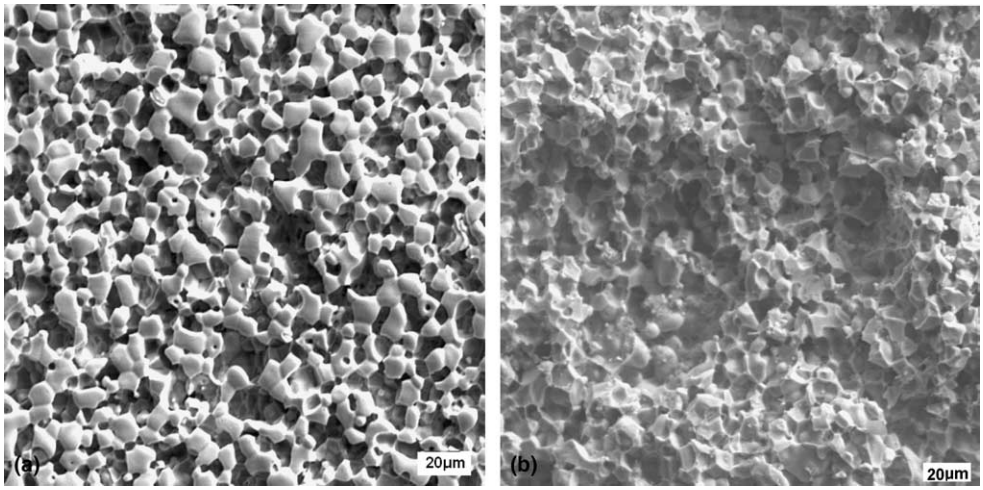

Fig. 10. Microstructure of MgO–ZrO_2 ceramic (50/50) at the completion of the acid-digestion experiment. Pellet outer surface (a) and as-fractured pellet surface (b) are shown. The porosity is due to dissolution of the free MgO phase.

caused by dissolution of the free MgO phase. Lack of the free MgO phase is evident on the outer surface and on the as-fractured surface of the pellet. A very thorough examination of the as-fractured surface detected two micron-sized MgO particles. These particles did not dissolve in the acid because they were completely encapsulated by the MgO–ZrO_2 solid solution phase. The particles became exposed only after the pellet was fractured for SEM examination.

X-ray diffraction (XRD) analysis was performed on the samples exposed to the nitric acid after the completion of the acid-digestion experiment. For this analysis the samples were ground into powder. Raw XRD patterns for nitric digested ceramic compositions are shown in Fig. 11. The patterns for as-fabricated ground ceramics are also included to emphasize the effect of acid digestion on the crystal structure. As evident from Fig. 11 the acid-digested ceramics lack the MgO phase. Therefore, the XRD

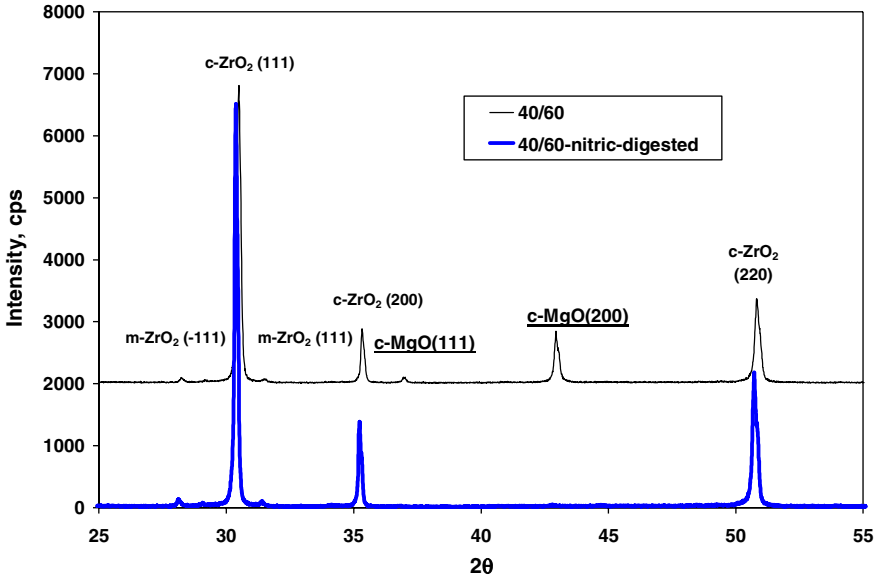

Fig. 11. Raw XRD pattern for nitric acid digested ceramic compositions shown in comparison with the pattern for as-fabricated ground ceramics. Nitric acid-digested ceramics lack the MgO phase. The effect is consistent for all three compositions, 60/40, 50/50 and 40/60.

confirms that an attempt to reprocess MgO–ZrO_2 based IMF using nitric acid will result in selective dissolution of the MgO phase leaving behind a ZrO_2 skeleton. (MgO present in the ZrO_2 phase as a solute remains intact). Thus, reprocessing of this fuel may be difficult using the nitric acid alone. Dissolution experiments with actual irradiated fuels will be needed to fully assess feasibility of reprocessing.

4. Conclusions

The study presented in this paper addressed two key issues associated with the feasibility of IMF based on MgO–ZrO_2 ceramics. The first issue is thermal transport properties. Thermal analysis, based on experimental and analytical techniques, established, that all investigated compositions of the product have thermal conductivities superior to that of UO_2 fuel. The second issue is solubility of MgO–ZrO_2 ceramics in nitric acid. Good solubility is key to successful fuel reprocessing. Ceramic dissolution experiments showed that only free MgO phase dissolves in the nitric acid, leaving behind a porous pellet consisting of MgO–ZrO_2 solid solution.

Further development of this novel fuel concept continues at the Idaho National Laboratory. It is being pursued as a part of the DOE Advanced Fuel Cycle Initiative's effort to evaluate transmutation in LWRs. Present activities at Idaho National Laboratory include fabrication and characterization of MgO–ZrO_2–Er_2O_3–PuO_2 fuel forms.

Experiments to fabricate ceramics containing PuO_2 powder are underway. The dispersion fuel option utilizing PuO_2 microspheres is being explored as well.

Acknowledgement

Dr S. M. Frank, Dr J. F. Jue and Dr T.P. O'Holleran of Idaho National Laboratory are gratefully acknowledged for performing XRD and SEM analyses. Sincere thanks to Mr A.P. Maddison for operating the laser flash diffusivity apparatus.

References

[1] P.G. Medvedev, Development of dual-phase magnesia–zirconia ceramics for light water reactor inert matrix fuel, Dissertation, Texas A&M University, 2004.
[2] P.G. Medvedev, S.M. Frank, T.P. O'Holleran, M.K. Meyer, J. Nucl. Mater. 342 (2005) 48.
[3] Standard Test Method for Thermal Diffusivity of Solids by the Flash Method, ASTM, E1461-01, West Conshohocken, PA, 2003.
[4] C. Ronchi, J.P. Ottaviani, C. Degueldre, R. Calabrese, J. Nucl. Mater. 320 (2003) 54.
[5] C. Degueldre, T. Arima, Y.W. Lee, J. Nucl. Mater. 319 (2003) 6.
[6] J.P. Ottaviani, Plutonium and Minor Actinides-Based Oxide Fuels Handbook, Note Technique LMPC n 2004-047, CEA, Cadarache, France, 2004.

[7] M.W. Chase Jr., J. Phys. Chem. Ref. Data, Monograph No. 9, 1998.
[8] D.Sh. Tsagareishvili, G.G. Gvelesiani, High Temp. 9 (1971) 588.
[9] C.E. Beyer, D.D. Lanning, C.L. Painter, FRAPCON-3: Modifications to Fuel Rod Material Properties and Performance Models for High-Burnup Application, Nuclear Regulatory Commission, Washington, DC, 1997, p. 3.8.